UNIVERSITÀ
DI PAVIA

Dipartimento di Scienze della Terra e dell'Ambiente

Direttore: Prof. S. Seno

Corso di Laurea Magistrale in

Geoscienze per lo Sviluppo Sostenibile

Age of Lunar Volcanism Recorded in the Clasts from the Lunar Breccia Meteorite NWA 12384

Relatore:

Prof. Matteo Alvaro

Correlatori:

Dott.ssa Murri Mara

Dott.ssa Stefania Righetto

Tesi di Laurea Magistrale

in Geoscienze per lo Sviluppo Sostenibile

di ANGELO PARAVELLA

matr. 544132

Anno Accademico 2024/25

Abstract

Age of Lunar Volcanism Recorded in the Clasts from the Lunar Breccia Meteorite NWA 12384

Angelo Paravella

Understanding the duration and diversity of lunar volcanism requires access to samples that record both early and late-stage magmatic activity. This study investigates the lunar polymict breccia meteorite NWA 12384, which provides a unique record of lithological diversity across the Moon's crust.

Fourteen lithic clasts were characterized using Scanning Electron Microscopy (SEM) and Energy Dispersive X-ray Spectroscopy (EDS), revealing a petrographic continuum from mafic cumulates to evolved basalts and felsic clasts. These lithologies reflect distinct magmatic sources and crystallization conditions, preserved within a breccia matrix that has been reshaped by impacts and regolith processes. One representative basaltic clast was selected for in situ Pb-Pb isotopic dating using Secondary Ion Mass Spectrometry (SIMS) on phosphate and feldspar grains.

The isotopic data yield a $^{204}Pb/^{206}Pb$ vs. $^{207}Pb/^{206}Pb$ isochron age of 3219 ± 13 Ma, placing its crystallization firmly within the Late Imbrian epoch. This age is consistent with a growing number of meteorite-based studies suggesting that volcanic activity on the Moon continued well after the primary phase of mare basalt emplacement recorded by Apollo samples. These findings support models of prolonged, spatially heterogeneous thermal evolution, potentially sustained by localized concentrations of radiogenic elements. They also reinforce the scientific value of lunar meteorites as records of magmatic and surface processes from across the Moon, offering critical constraints that mission-returned samples alone cannot provide.

Keywords: NWA 12384 Lunar meteorite, Pb-Pb dating, SIMS, Lunar volcanism, Breccia, SEM-EDS mapping, isotope

Popular Science Summary

Lunar rocks aren't only found on the Moon. Some of them have landed on Earth as meteorites, after being blasted off the lunar surface by ancient impacts. This project looked at one such meteorite, named NWA 12384, which contains tiny rock fragments, called breccias, from deep inside the Moon. Using high-powered microscopes and precise instruments, the study revealed a mixture of rock types that formed through volcanic activity billions of years ago. One fragment was found to have formed over 3.2 billion years ago, hundreds of millions of years after the major volcanic events recorded by Apollo mission samples, which mostly range from 3.9 to 3.5 billion years ago. This means that, beneath its quiet, cratered surface, the Moon was still alive with hidden heat for much longer than expected. Meteorites like this help us understand parts of the Moon that no previous exploration has ever visited, and give us a richer picture of our planet’s satellite history.

Table of Contents

1. Introduction

1.1 The Study of Lunar Meteorites

Lunar meteorites open an exceptional window into the Moon's broader geological history. Unlike the Apollo and Luna mission samples, which were collected from specific, geologically constrained locations (Joy & Arai, 2013), meteorites provide access to materials ejected randomly across the lunar surface, often from regions that have never been visited directly. This randomness is, paradoxically, their greatest scientific strength (Papike et al., 1998).

Through these meteorites, we gain access to a more diverse and representative spectrum of lunar crustal materials. By combining petrography, geochemistry, and isotopic dating, these samples have been instrumental in refining our understanding of lunar magmatism, regolith evolution, and planetary chronology (Snape et al., 2016).
For example, Merle et al. (2020) used Pb-Pb isotopic dating to identify temporally distinct magmatic episodes in lunar breccias, revealing that volcanism extended well beyond the primary mare basalt phase. Similarly, Yen et al. (2024) has studied a fragment of NWA 12384 and identified a wide range of lithologies, including evolved basalts and felsic components, along with a Late Imbrian crystallization age of ~3220 Ma, supporting prolonged and heterogeneous volcanic activity. Ultimately, studies like these help reconstruct a more global and time-resolved picture of lunar geological evolution.

1.2 Importance of Lunar Breccias

Polymict breccias, complex mixtures of fragmented rocks fused together by impacts, act as natural time capsules that record the geological evolution of the Moon (Papike et al., 1998; Joy & Arai, 2013). They combine highland anorthosites (crustal rocks), mare basalts (volcanic infill of lunar basins), and impact melts. Each clast within a breccia retains a piece of lunar history, whether magmatic, metamorphic, or impact-related (Hiesinger et al., 2011).

Analyzing these clasts individually allows the disentangling of overlapping processes that occurred on the Moon. The microstructures and mineral chemistry preserved in each fragment provide insight into the sequence and nature of lunar volcanism, brecciation, and regolith evolution (Yen et al., 2024; Merle et al.,

2020). Dating these components separately allows reconstruction of distinct events in lunar history as geochronological data points.\

1.3 NWA 12384 Meteorite: A Scientific Opportunity

Among known lunar breccias, Northwest Africa (NWA) 12384 (Figure 1) stands out as an unusually pristine and compositionally diverse sample. It was recovered in 2018 near Bir Anzarane, Western Sahara (administered by Morocco), and acquired by meteorite collector Luc Labenne, who submitted it for classification. The Meteoritical Society officially approved it in 2019 as a polymict lunar breccia with a total known weight of 582 grams (Irving & Kuehner, 2019). The sample consists of a fine-grained, partially melted matrix enclosing clasts ranging from primitive mafic cumulates to evolved basaltic and feldspathic fragments.

This lithological variety reflects a broad range of lunar magmatic and impact processes, making NWA 12384 an ideal target for combined petrographic, geochemical, and chronological investigation. A prior study by Yen et al. (2024) analyzed a separate fragment from the same meteorite, documenting multiple lithologies and dating a basaltic clast to ~3220 Ma. The present work focuses on a previously uncharacterized fragment of the breccia, offering an opportunity to independently test and expand upon those findings using a different portion of the same parent body.

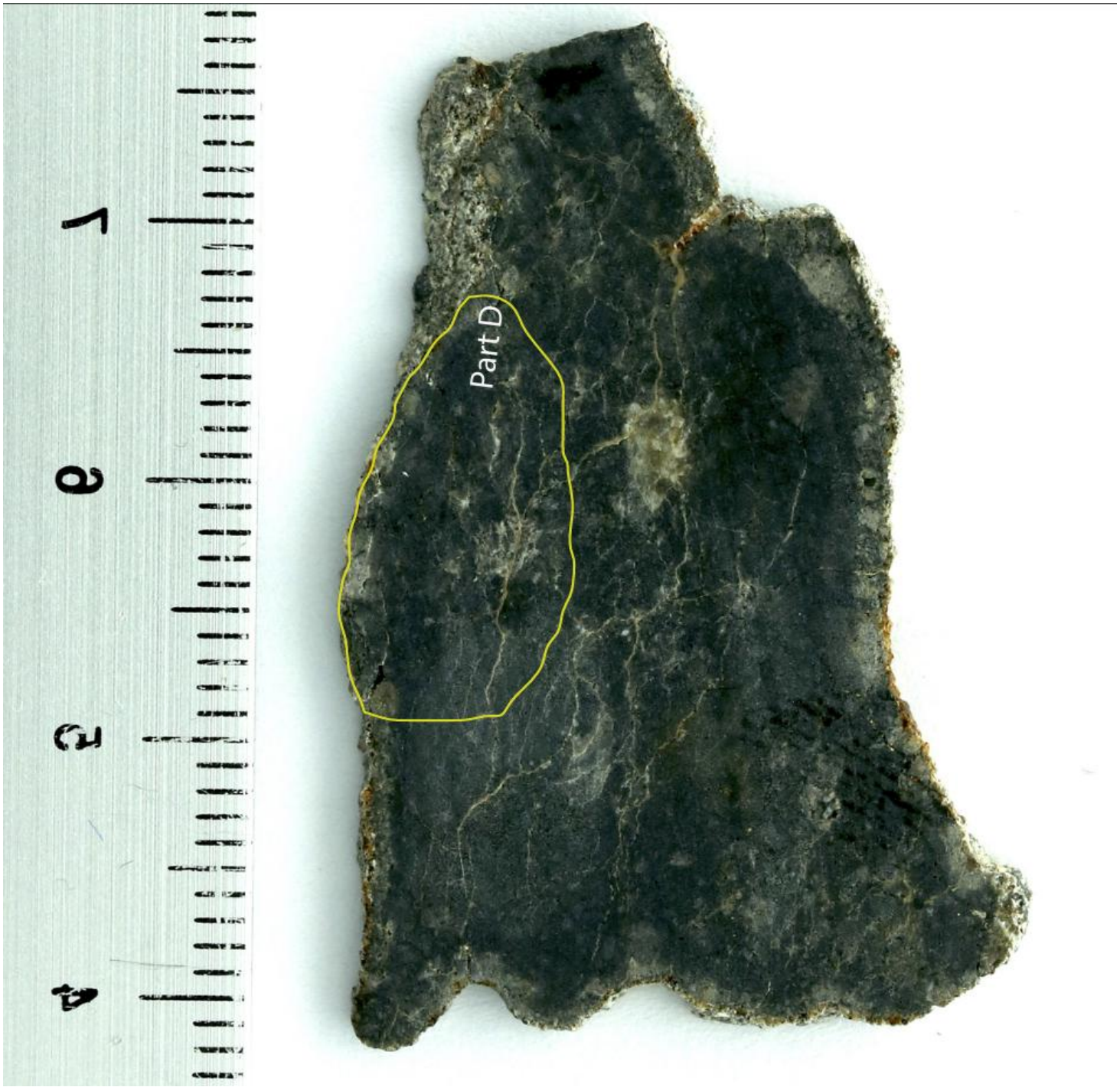

Figure 1, Photograph of the NWA 12384 lunar meteorite, classified as a polymict breccia. Image edited from Luc Labenne.

2. Aims

This thesis is designed to contribute a multifaceted understanding of lunar volcanic history as preserved in the clasts of NWA 12384. The sample is a large portion of the meteorite that has been cut into several fragments. Yen et al. (2024) analyzed one of these fragments, and the present study investigates another, previously uncharacterized portion.
The project focuses on the following research objectives:

First, to analyze the lithological diversity and geochemical characteristics of the previously uncharacterized “Area D” of the NWA 12384 meteorite (Figure 2), thereby expanding the mineralogical and chronological dataset available for this breccia (Yen et al., 2024).

Second, to conduct detailed mineralogical and geochemical characterization of basaltic clasts using Scanning Electron Microscopy (SEM) and Energy-Dispersive X-ray Spectroscopy (EDS), identifying mineral phases and assessing their textures and associations (Ortega et al., 2022).

Third, to distinguish major, minor, and accessory mineral assemblages, with particular emphasis on those preserving primary magmatic features or post-magmatic impact-related modifications (Papike et al., 1998).

Fourth, to perform in situ Pb-Pb isotopic dating of U- and Pb-bearing minerals such as zircon, baddeleyite, phosphate, potassium feldspar, and sulphide using Secondary Ion Mass Spectrometry (SIMS), anchoring the sample within the broader lunar geological timeline (Snape et al., 2016; Merle et al., 2020).

Finally, to interpret the resulting geochemical and chronological data in the context of lunar magmatic evolution, impact history, and regolith development, with the goal of contributing in refining benchmarks for lunar volcanism and understanding the Moon’s thermal evolution in its later geological history (Hiesinger et al., 2011; Norman, 2009).

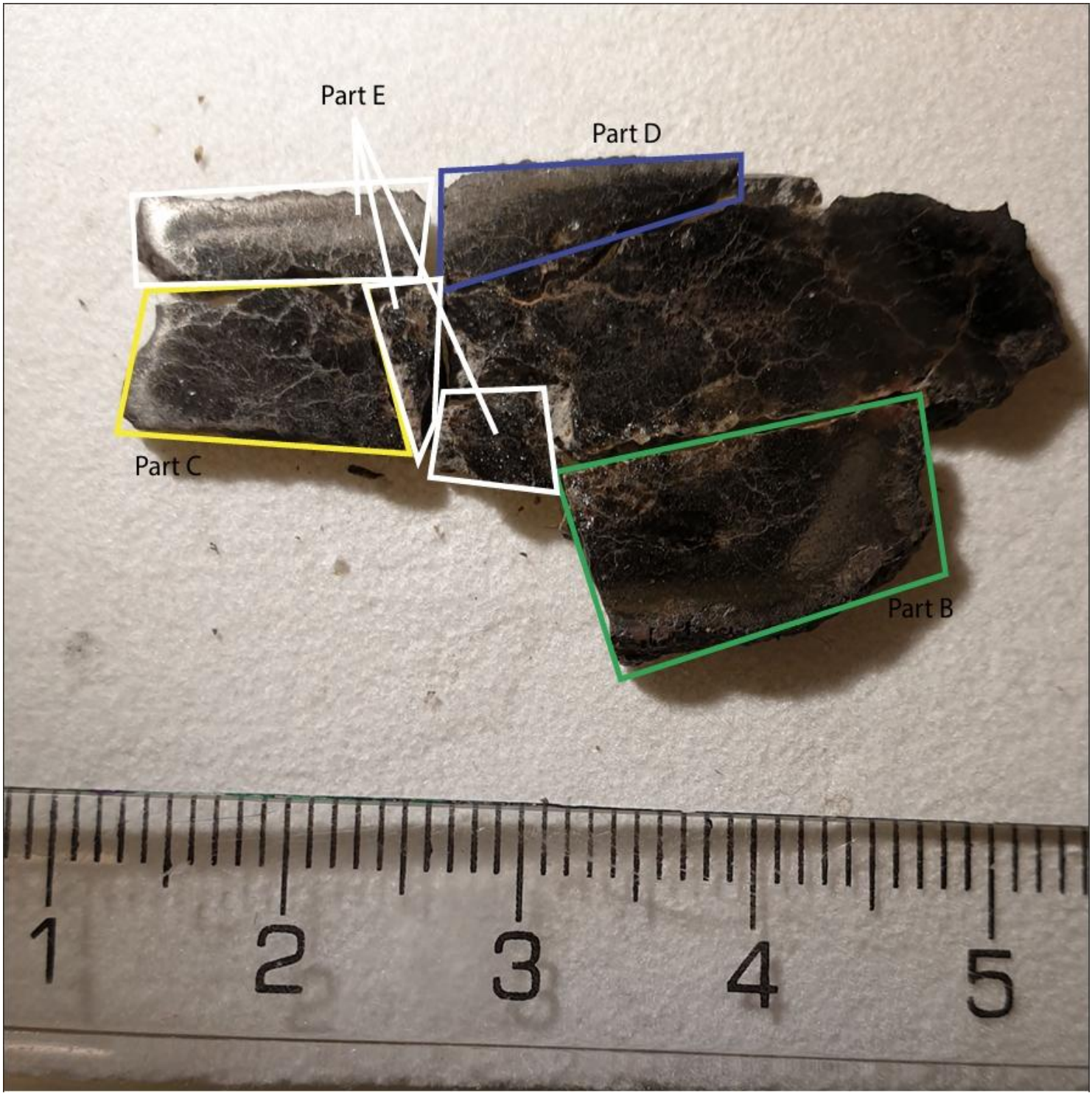

Figure 2, Macroscopic view of the NWA 12384 fragment used in this study, Merle et al., 2020.

3. Background

3.1 The Moon's Geological Evolution

The Moon's geological evolution began with a colossal impact between the early Earth and a Mars-sized body, often referred to as Theia, around 4.5 billion years ago. This impact likely gave rise to the Earth–Moon system (Canup, 2004). Following its formation, the Moon underwent rapid planetary differentiation, resulting in the crystallization of a global magma ocean. As the magma ocean solidified, it produced a primary crust dominated by anorthositic rocks and a mantle composed of early mafic cumulates (Shearer & Papike, 1999).

Subsequent lunar history was marked by repeated episodes of volcanic activity that produced the vast basaltic plains known as the lunar maria, as well as extensive impact modification due to continued meteoritic bombardment (Hiesinger et al., 2011; Norman, 2009). These impacts reshaped the surface, generating basin structures, regolith, and polymict breccias. Studying this evolution relies heavily on the examination of both pristine magmatic rocks and impact-modified materials, particularly those preserved in lunar meteorites, which offer access to unsampled regions of the Moon’s crust (Joy & Arai, 2013).

3.2 Lunar Volcanism and Magmatism

Volcanism on the Moon was not a single, isolated event but rather a series of magmatic episodes that spanned billions of years, from approximately 4.3 to 1.2 billion years ago (Hiesinger et al., 2011; Snape et al., 2016). This long-lived activity produced a wide variety of basaltic compositions, which reflect differences in mantle source regions, degrees of partial melting, and depth of origin (Shearer & Papike, 1999).

Lunar basalts are commonly grouped into three main compositional types: low-Ti, high-Ti, and KREEP-rich basalts. High-Ti and KREEP basalts are typically older, whereas low-Ti basalts are generally younger and more voluminous (Hiesinger et al., 2011). Studies by Merle et al. (2020) and Yen et al. (2024) indicate that these geochemical variations correspond to episodic magmatic activity, controlled by regional differences in mantle composition and thermal evolution.

3.3 Lunar Breccias and Impact Processes

Lunar breccias are among the most complex and revealing geological materials on the Moon. Formed during high-energy impact events, they consist of rock fragments from diverse origins that have been mechanically mixed and thermally altered (Papike et al., 1998; Joy & Arai, 2013). These rocks preserve both pristine crustal components and the signatures of intense post-formational processing, including shock metamorphism, melting, and recrystallization.

In this sense, breccias function as stratified geological archives. They capture evidence of surface gardening, meteoritic bombardment, and deep crustal excavation that occurred over billions of years (Norman, 2009). By examining individual clasts within breccias, it is possible to reconstruct a localized but multi-phase history of magmatism, metamorphism, and impact processes, offering insights into both regional and temporal evolution across the Moon's surface.

3.4 Previous Studies on Lunar Meteorites

Over the past two decades, lunar meteorites have significantly transformed our understanding of the Moon's magmatic and thermal evolution. In contrast to the spatially restricted Apollo and Luna samples, meteorites are believed to originate from diverse and previously unsampled regions of the lunar crust. Their random ejection and delivery to Earth provide access to a broader geological context, including terrains not explored by landed missions (Joy & Arai, 2013; Papike et al., 1998).

Merle et al. (2020) conducted in situ Pb-Pb dating of phosphates and feldspars in several lunar meteorites, including breccias such as NWA 4734 and members of the NWA 773 clan. Their study revealed a series of temporally discrete magmatic events, with ages clustering around 3900 Ma and extending to as young as ~2900 Ma. These results confirmed that lunar magmatism was not only prolonged but also episodic, with substantial thermal evolution long after the major period of mare basalt emplacement. Additionally, Merle et al. noted significant isotopic heterogeneity within individual clasts and breccias, suggesting repeated mixing of crustal materials with different magmatic histories.

Building on this approach, Yen et al. (2024) analyzed a separate fragment of NWA 12384 using SEM, EDS, and SIMS(figure 3). Their study documented a diverse range of clasts, including Fe-

Ti-rich basalts, primitive mafic cumulates, and evolved feldspathic fragments. One basaltic clast yielded a Pb-Pb crystallization age of ~3220 Ma, placing it in the Late Imbrian epoch. This result demonstrated that volcanic activity persisted in localized magmatic provinces well after the main Apollo-era volcanic peak. Yen et al. also noted well-preserved primary textures in several clasts, indicating limited shock overprinting and making NWA 12384 an especially valuable sample for geochronology.

Together, these studies provide critical context for the present investigation. The discovery of similarly aged and texturally intact clasts within a different portion of the same meteorite, such as Clast 1 in this study, reinforces the interpretation that NWA 12384 preserves a geochemically and temporally diverse record of late-stage lunar magmatism.

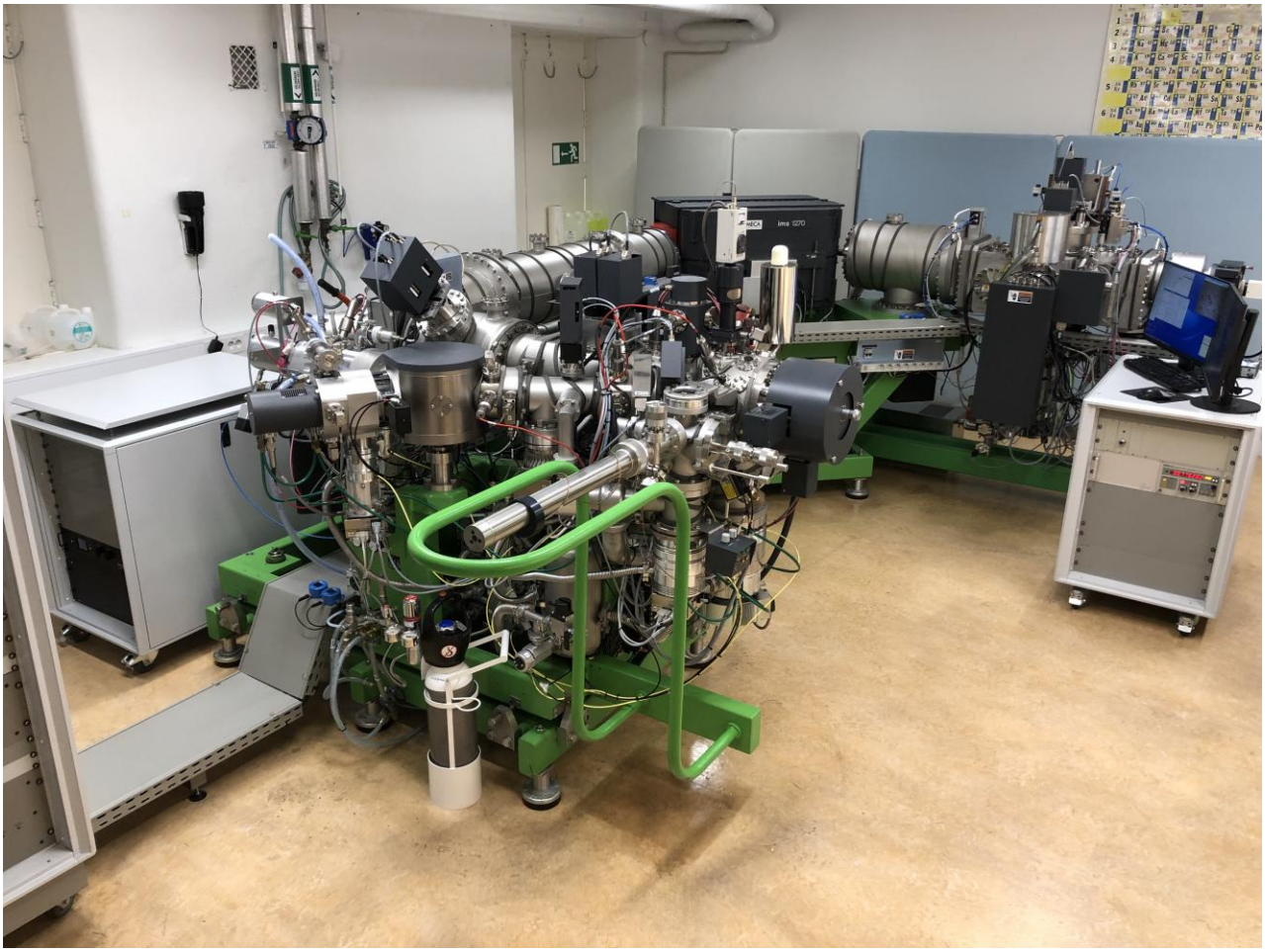

Figure 3, The CAMECA IMS 1280-HR Secondary Ion Mass Spectrometer (SIMS) at the Swedish Museum of Natural History (NRM), used for Pb-Pb isotopic analyses.

4. Methodology

4.1 Sample Preparation

Preparing the NWA 12384 samples for analytical work required meticulous effort to preserve both chemical integrity and microstructural detail. Thick sections were created by precision cutting and embedding the resulting fragments in epoxy, followed by careful polishing to expose fresh internal surfaces (Yen et al., 2024).

To prevent contamination or thermal alteration, only non-reactive polishing agents were used, and care was taken to minimize heat buildup during grinding. The sections were mounted on glass slides and coated with a conductive layer of carbon to ensure imaging stability and signal consistency during electron beam analysis (Ortega et al., 2022). Each mount was pre-screened under reflected light to identify large, intact clasts with minimal weathering or brecciation for subsequent microanalytical work.

4.2 SEM and EDS Mapping

Scanning Electron Microscopy (SEM) was employed to obtain high-resolution images of mineral textures and phases within the NWA 12384 breccia. Backscattered electron (BSE) imaging was used to distinguish mineral phases based on atomic number contrast, while Energy-Dispersive X-ray Spectroscopy (EDS) enabled semi-quantitative elemental analysis of each clast (Ortega et al., 2022; CAMECA EPMA).

All SEM-EDS analyses were conducted at the Swedish Museum of Natural History (NRM) using a JEOL JXA-8530F field emission electron probe microanalyzer (EPMA, figures 4-5). The instrument operated at an accelerating voltage of 15 kV and a beam current of 10 nA. Elemental maps were acquired with a dwell time of 300 μs per pixel, using a beam diameter of approximately 1 μm. Mapping resolution typically ranged from 512 × 384 to 1024 × 768 pixels, depending on the size of the clast.

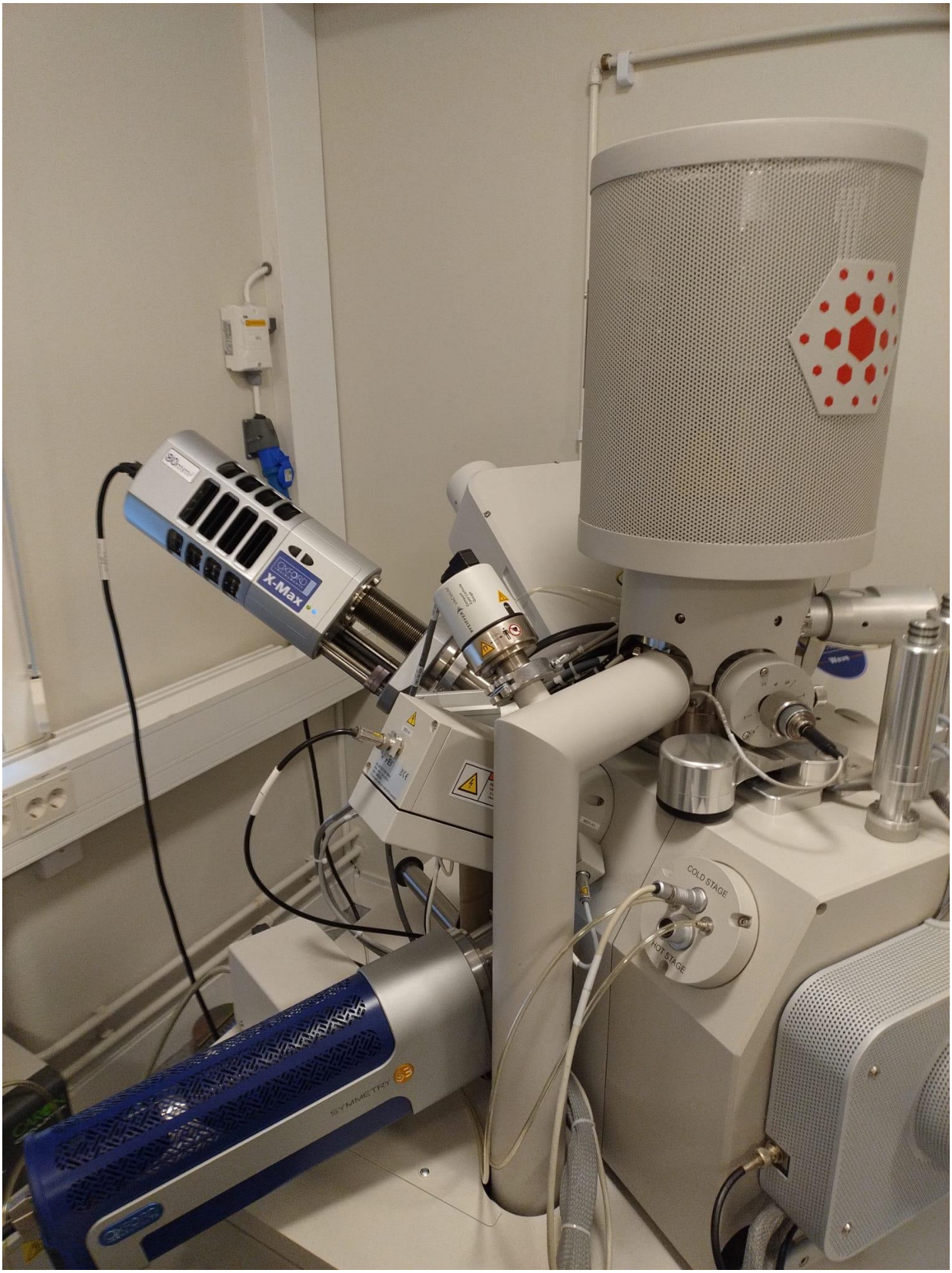

Figure 4, The JEOL JXA-8530F Electron Probe Microanalyzer (EPMA) at NRM used for SEM and EDS mapping in this study.

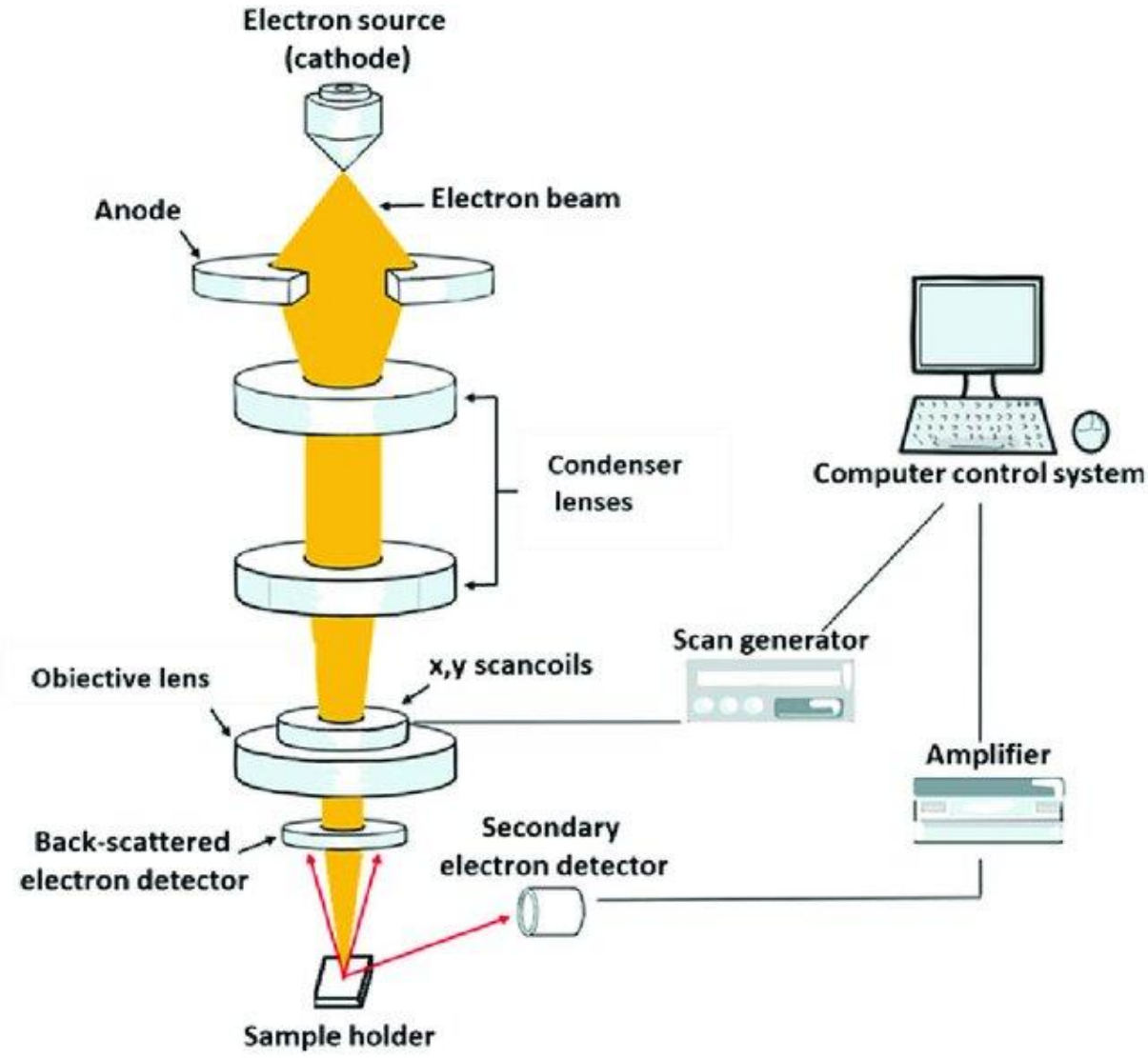

Figure 5, Schematic diagram of the EDS analytical method, Ortega et al. (2022).

EDS mapping focused on key elements including Al, Fe, Mg, Ca, Ti, and Cr, providing information on the spatial distribution of mineral phases and zoning patterns (Figures 6–9). These maps were instrumental in identifying clasts with minimal alteration and selecting target minerals for in situ SIMS analysis. All images were post-processed using Adobe Illustrator for enhanced contrast and layering of element-specific data.

Figure 6, Summary of major chemical phases identified by EDS in the NWA 12384 sample, screenshot from Adobe Illustrator.

Figure 7, Base EDS layer map used for the chemical analysis

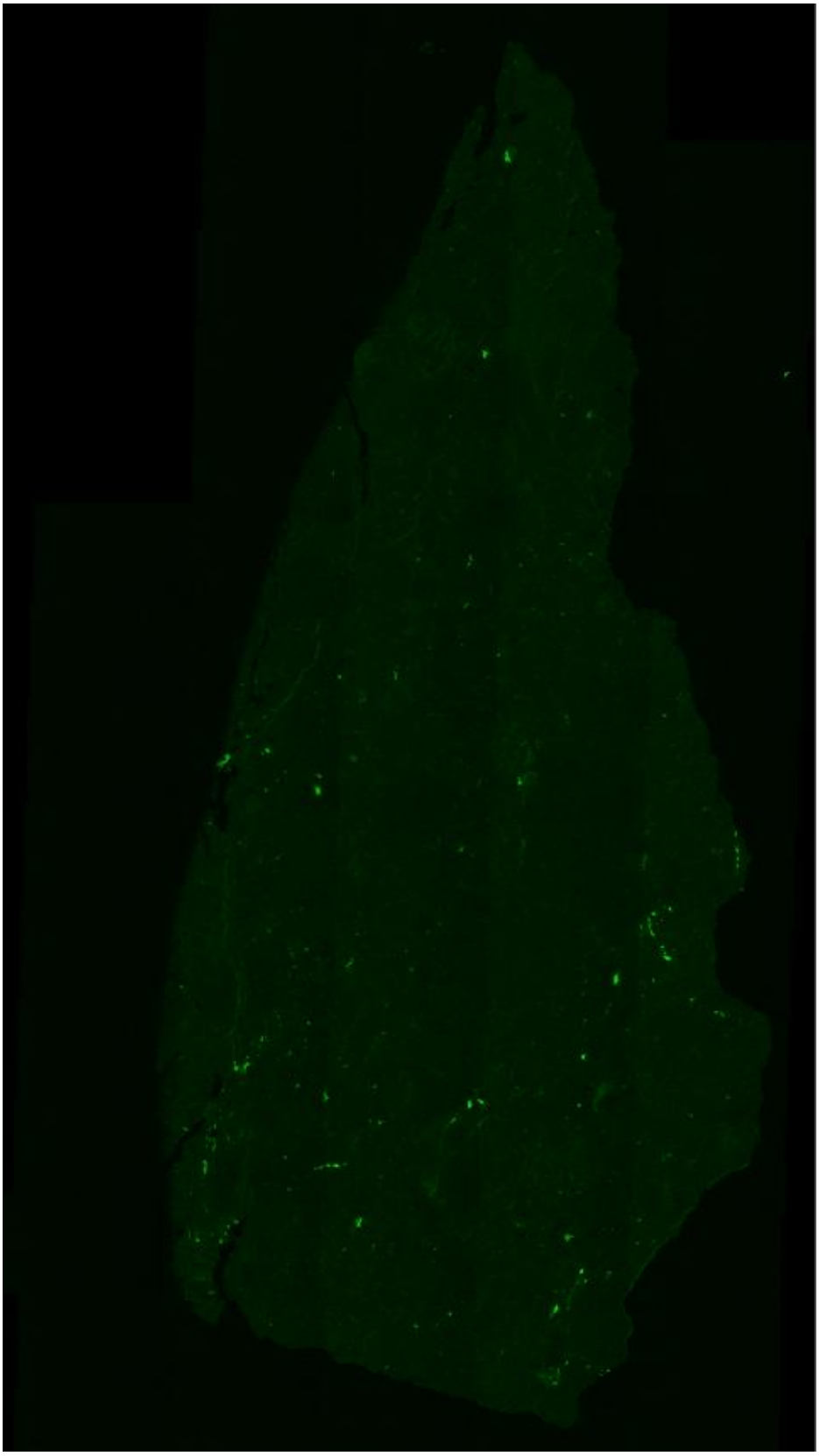

Figure 8, EDS elemental map showing the distribution of potassium (K)

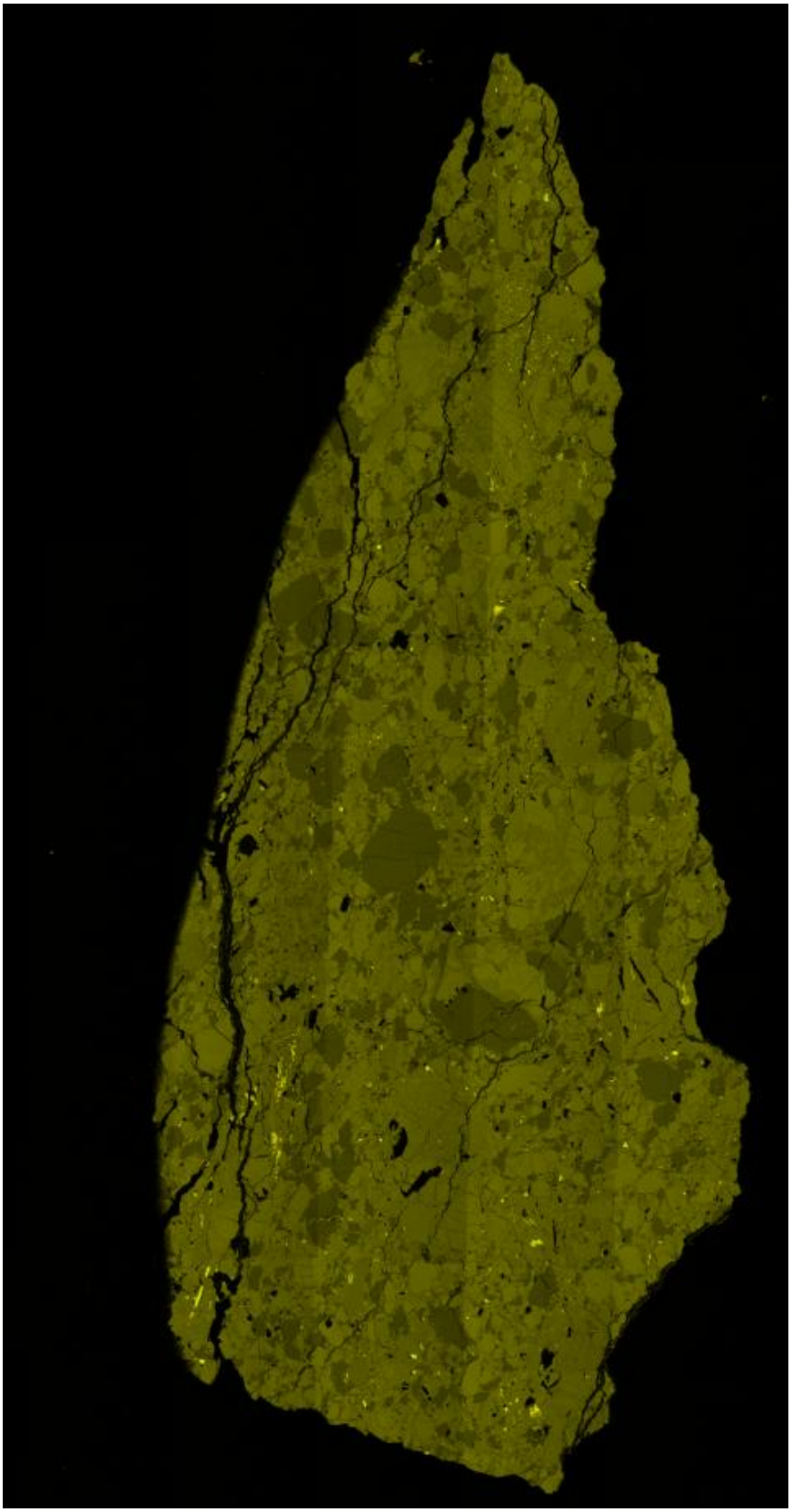

Figure 9, EDS elemental map showing the distribution of silicon (Si)

4.3 In situ Pb-Pb dating by Secondary Ion Mass Spectrometry (SIMS)

In situ Pb-Pb isotopic measurements were performed using a CAMECA IMS 1280-HR instrument (figure 10) at the Swedish Museum of Natural History in Stockholm (NRM). This high-resolution SIMS system is equipped with dual primary ion sources, cesium (Cs^+) and oxygen (O_2^+), allowing for flexible analysis of both electronegative and electropositive elements at high spatial resolution (CAMECA SIMS, n.d.)

The oxygen primary ion beam (O_2^+), generated by a duoplasmatron source, was used for most Pb-Pb analyses due to its high efficiency in generating negative secondary ions from phosphate and feldspar phases.
In selected cases, a Cs^+ beam was employed to enhance the yield of positive secondary ions from U-bearing minerals. Spot analyses were conducted with a beam diameter of ~10 μm and a typical current of ~1.5 nA, achieving sufficient depth profiling without ablating entire grains.

Pb isotopic data were collected from U- and Pb-bearing minerals such as phosphate, potassium feldspar, and, where present, zircon or baddeleyite. Each spot analysis measured ^{204}Pb, ^{206}Pb, and ^{207}Pb, with mass fractionation corrections applied using internal standards. Special care was taken to avoid inclusions and altered domains, and all targets were pre-screened by SEM-EDS to ensure suitability. This configuration (figure 10) ensures high sensitivity and precision in isotopic measurements, crucial for interpreting the magmatic history recorded in the lunar breccia meteorite NWA 12384.

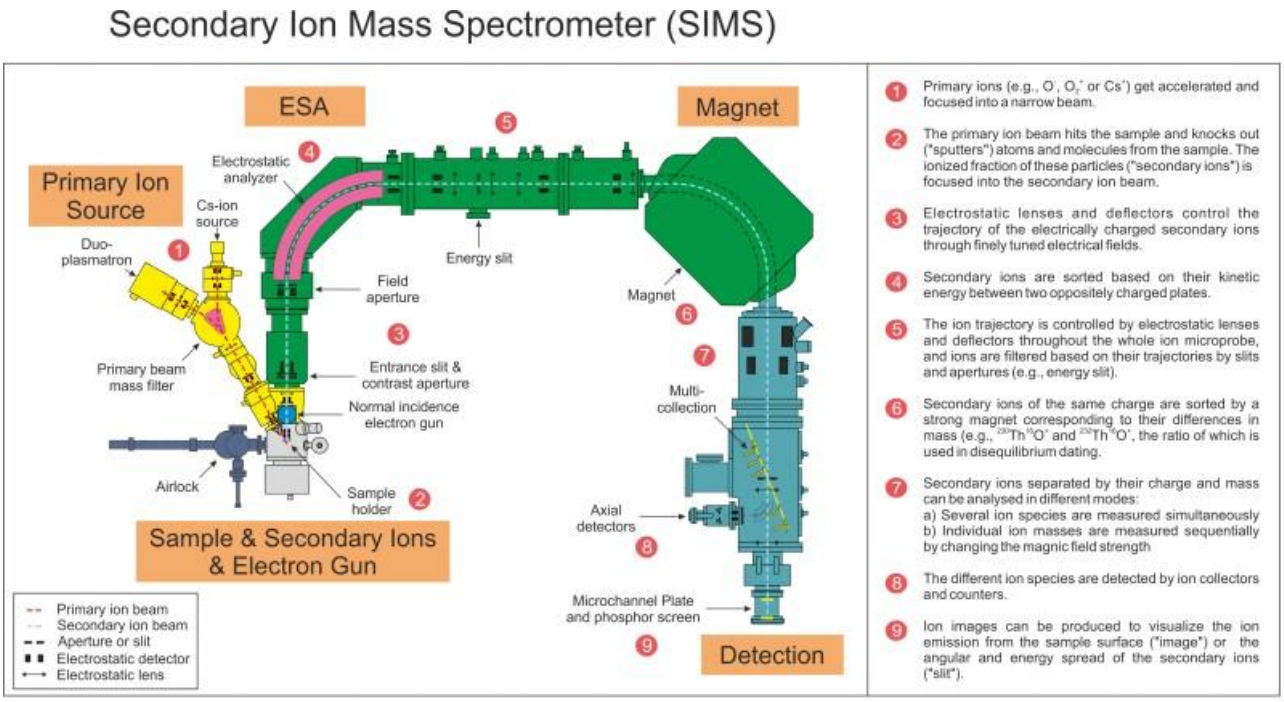

Schematic diagram of the CAMECA IMS 1280-HR

Figure 10, Schematic Diagram for the SIMS, from CAMECA's website

In this study, Pb isotopic measurements were conducted in situ using Secondary Ion Mass Spectrometry (SIMS) on U- and Pb-bearing minerals. This technique involves sputtering the surface of U- and Pb-bearing minerals with a focused primary O^- ion beam to liberate secondary ions for mass analysis (figure 11).

A key advantage of this technique is the ability to construct isochrons by plotting $^{204}Pb/^{206}Pb$ against $^{207}Pb/^{206}Pb$. These two-component linear regressions help correct for common Pb and allow robust age calculation even in minerals with complex or mixed Pb reservoirs. In this study, isochron construction followed the method outlined by Ludwig (2008), using the Isoplot 3.60 software, which incorporates analytical uncertainties and inter-spot scatter into the regression. Model ages were calculated with 95% confidence intervals.

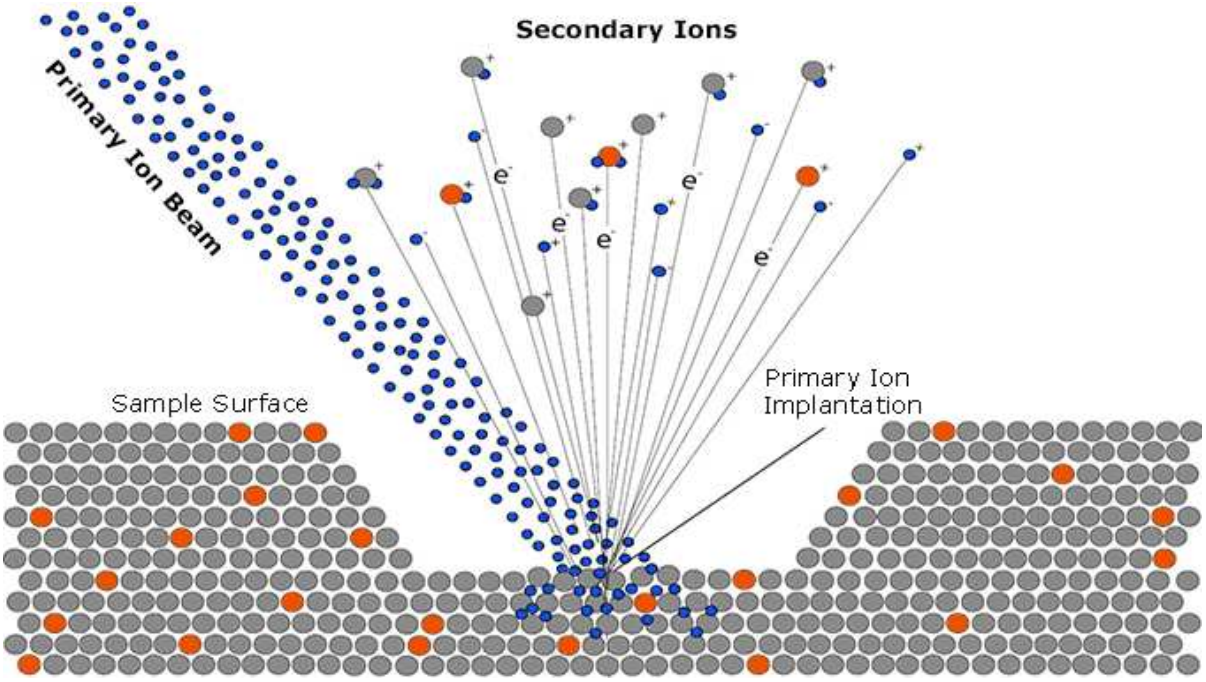

Figure 11, The principle sample interaction when applying the SIMS technique, from CAMECA's Website

To address possible terrestrial contamination, the measured Pb isotopic compositions were compared to the common Pb model of Stacey and Kramers (1975). Data points deviating from the expected radiogenic trend were examined and filtered to improve regression accuracy (figure 12). Ultimately, the resulting isochron age provides a reliable estimate of the crystallization time of the clast analyzed, offering insight into the timing of volcanic activity recorded in the NWA 12384 breccia (Merle et al., 2020; Yen et al., 2024).

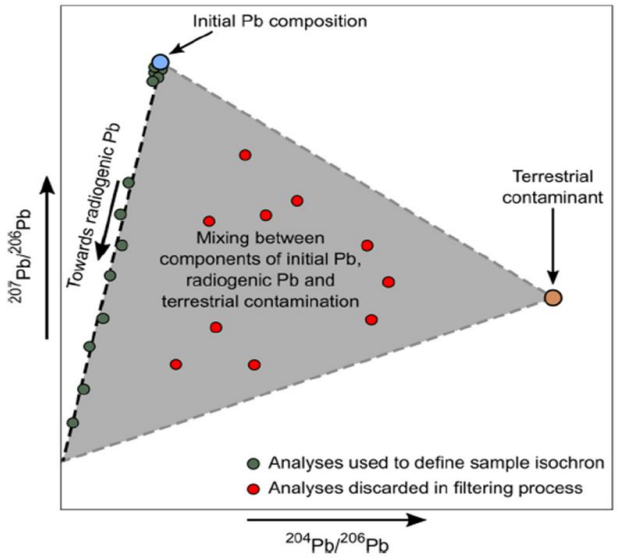

Figure 12, U-Pb processed data (Snape et al 2016)

4.4 Data Processing and Interpretation

SEM Imaging

The raw SEM-EDS data were carefully analyzed to characterize mineralogy, alteration features, and textural relationships among phases. Minerals were identified based on their elemental composition, allowing for distinction between primary igneous assemblages and secondary alteration products. Elemental maps and backscattered electron (BSE) images were used to assess zoning, recrystallization, and fracture patterns, helping to inform clast selection for isotopic analysis (Ortega et al., 2022; Yen et al., 2024).

SIMS data processing

SIMS data consisted of multiple spot measurements across U-bearing mineral phases, primarily phosphates and feldspars. Visibly altered zones were excluded. Raw isotopic ratios for ^{204}Pb, ^{206}Pb, and ^{207}Pb were corrected for instrumental mass fractionation and filtered to remove outliers or contamination-affected analyses. Isochron regression was conducted using the Isoplot 3.60 software (Ludwig, 2008), which accounts for both analytical uncertainties and scatter within the dataset. This software produced linear regressions with confidence intervals and generated model ages based on the $^{204}Pb/^{206}Pb$ vs. $^{207}Pb/^{206}Pb$ plot.

Accessory minerals such as sulphides and rare zircon grains were noted but not consistently present across clasts. Data from the best-preserved and compositionally appropriate phases were used to construct the final age model.

5. Results

5.1 Petrography of NWA 12384

The NWA 12384 meteorite is a polymict breccia composed of a heterogeneous mixture of lithic clasts, mineral fragments, and interstitial material set within a fine-grained matrix. The clasts exhibit a wide range of lithologies, including subophitic basalts, Fe-Ti-rich evolved melts, mafic cumulates, Cr-spinel-bearing gabbros, and felsic or feldspathic components (Yen et al., 2024). Their sizes range from sub-millimeter grains to several millimeters across, and they vary in shape from angular to sub-rounded, reflecting different histories of fragmentation and transport.

The matrix is dark, fine-grained, and partially glassy in appearance, consistent with an origin as an impact-generated melt. It contains abundant comminuted mineral fragments, vesicular textures in places, and a groundmass that often exhibits flow-like alignment of clastlets and plagioclase laths. In some areas, interstitial melt has crystallized into microcrystalline phases, suggesting rapid quenching, while in others it remains partially devitrified or glassy.

Interstitial textures are common within larger clasts, often showing late-stage crystallization features such as graphic intergrowths between plagioclase and silica-rich glass or localized enrichment in phosphates and Fe-Ti oxides. These interstitial domains frequently border primary igneous textures, indicating incomplete crystallization at the time of brecciation.

Impact textures are pervasive across the sample. These include shock veins, melt pockets, and recrystallization rims around individual mineral grains. Some clasts show evidence of granular deformation and mosaicism in plagioclase, confirming moderate to high shock conditions.

Alteration textures, while generally minor, are present in some clasts. These include narrow Ca-P-rich veins interpreted as secondary phosphate mobilization, Fe-oxide halos around fractures, and limited hydration along cracks. These features may reflect terrestrial weathering or post-shock metasomatism, though their extent appears minimal compared to fresher phases.

Overall, NWA 12384 exhibits complex textural relationships that reflect a long and multi-phase history, combining primary magmatic crystallization with subsequent brecciation, impact processing, and minor alteration. These petrographic features provide critical context for interpreting the chemical and isotopic data presented in subsequent sections.

5.2 Elemental Mapping

Elemental mapping of selected clasts using EDS revealed heterogeneous yet informative patterns in the distribution of major and minor elements. Aluminum and calcium were strongly concentrated in plagioclase-rich regions, while iron and titanium were most abundant in oxide phases, such as ilmenite and titanomagnetite. These patterns are consistent with typical crystallization trends observed in lunar basaltic rocks (Papike et al., 1998; Yen et al., 2024).

Magnesium was often inversely correlated with iron, reflecting a compositional gradient from more primitive to evolved lithologies. Chromium and vanadium showed consistent association with spinel-group minerals and Fe-oxides. Phosphorus was localized in discrete phosphate phases, typically apatite, found in late-stage interstitial melt pockets. These minerals provided the primary targets for isotopic dating via SIMS (see Section 4.3).

Elemental distribution maps (Figure 13) were critical in distinguishing between primary magmatic textures and secondary alteration zones. In a few cases, fractures were observed to contain elevated Ca and P, suggesting possible terrestrial alteration. However, overall alteration appeared minimal, and most clasts retained their primary igneous mineralogy and texture. This chemical mapping was essential for identifying minimally altered regions suitable for in situ isotopic analysis.

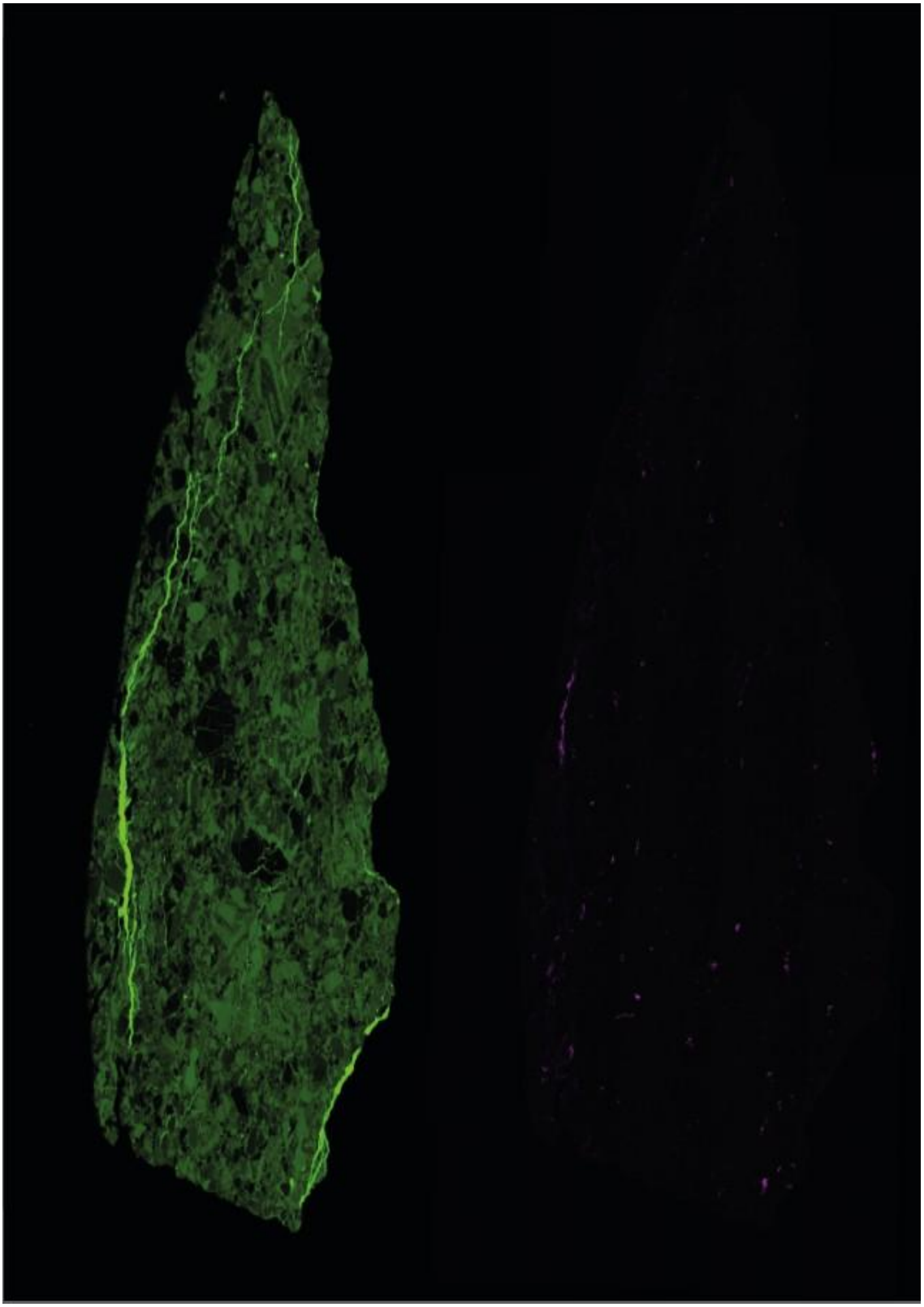

Figure 13, Elemental maps comparing the distribution of calcium (left) and phosphorus (right)

5.3 Classification of Basaltic Clasts

The clasts within NWA 12384 are petrographically diverse and can be categorized into several broad lithological types based on their textures, mineralogy, and geochemical characteristics (Yen et al., 2024). This classification helps to distinguish between different magmatic sources and crystallization histories recorded in the breccia:

- Subophitic Basalts: These clasts exhibit intergrown plagioclase and pyroxene forming subophitic textures, consistent with crystallization from relatively evolved magmas under moderate cooling rates (Papike et al., 1998). They are among the most common lithologies in the sample.

- Primitive Mafic Cumulates: These clasts are dominated by Mg-rich olivine and pyroxene, with low feldspar content. Their mineralogy and textures suggest crystallization from early, high-temperature magmas derived from the lunar mantle.

- Fe-Ti Oxide-Rich Basalts: Characterized by high abundances of ilmenite and titanomagnetite, these clasts represent evolved magmas that underwent late-stage differentiation, likely from iron- and titanium-enriched melts (Merle et al., 2020).

- Cr-rich Spinel-Bearing Clasts: These contain abundant chromium-bearing spinel phases, often in association with pyroxenes and plagioclase. Their textures point to a gabbroic or cumulate origin, possibly linked to layered magmatic intrusions within the lunar crust (Snape et al., 2016).

- Felsic Clasts: Identified by high Al and low Fe content, these fragments may represent evolved intrusive materials or residual melt pockets formed during extreme fractional crystallization (Yen et al., 2024).

This classification scheme aids in interpreting the thermal and magmatic diversity recorded within the NWA 12384 breccia and forms the basis for selecting representative clasts for further geochemical and isotopic analysis.

5.4 Description of Individual Clasts (1–14)

A wide range of lithologies is observed among the 14 analyzed clasts, reflecting diverse magmatic, impact, and alteration histories. SEM imaging and EDS mapping were used to characterize mineralogy, texture, zoning, and deformation features. The mineral percentages below are approximate volumetric estimates based on phase abundance in BSE images and elemental maps.

Clasts 1, 2, and 4 are subophitic basalts composed of intergrown plagioclase and low-Ca pyroxene, with interstitial phosphate and potassium feldspar phases. The clasts preserve a sharp igneous texture with minimal fracturing and no observable shock overprints. Phosphates appear as small, bright grains in BSE and are confirmed by P-rich zones in EDS maps (Figure 14). These textures suggest moderate cooling and crystallization in an extrusive or shallow intrusive setting.

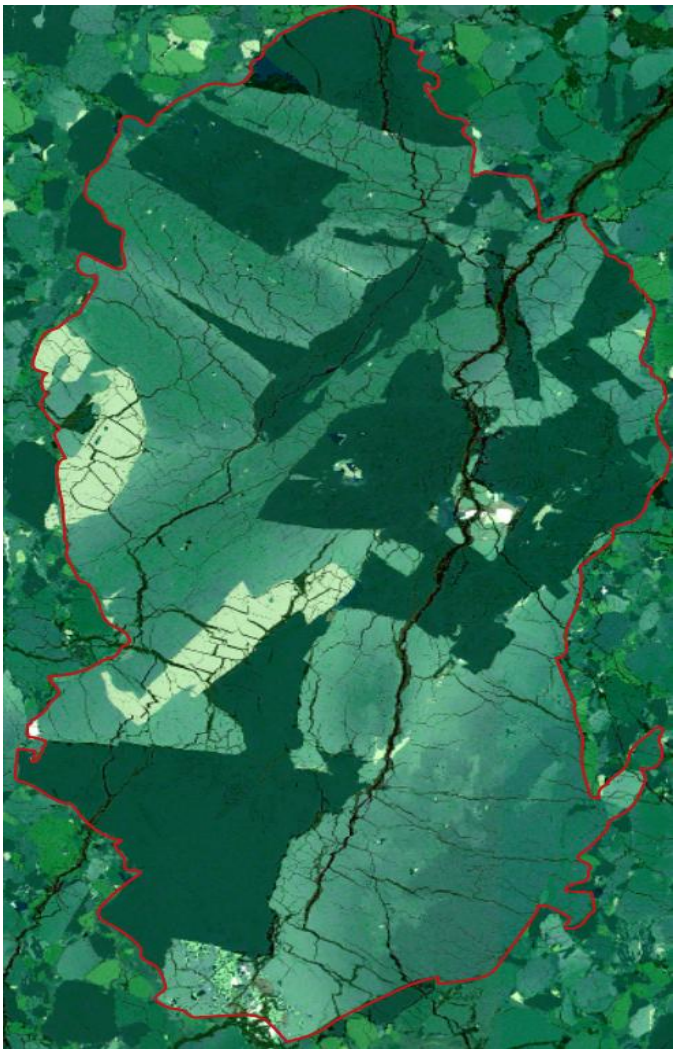

Figure 14, BSE image of Clast 2, a subophitic basalt

Clast 3 is a fine-grained Fe-Ti-rich basalt characterized by iron oxides (~17%) finely distributed within a pyroxene- and plagioclase-dominated matrix (Figure 15). The Fe oxides are easily identifiable in BSE and EDS images due to their high atomic number contrast and Fe-Ti enrichment. The texture is homogeneous with no vesiculation or zoning, and no alteration halos are observed. The absence of deformation features suggests preservation of primary magmatic textures.

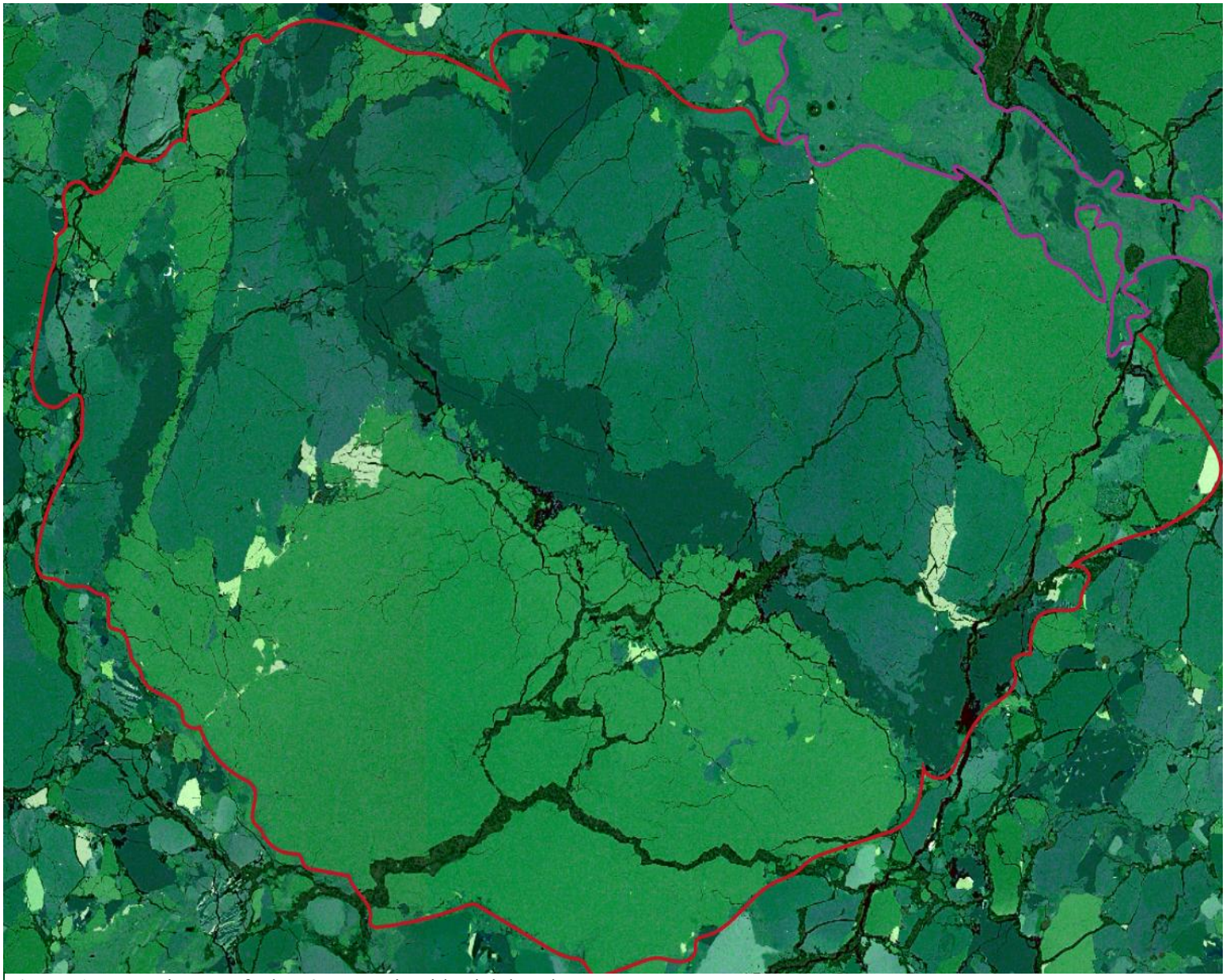

Figure 15, SEM image of Clast 3, a Fe-Ti oxide-rich basalt

Clast 5 displays a porphyritic basaltic texture, consisting of large feldspar phenocrysts (up to 700 μm) surrounded by a fine-grained Fe-rich matrix (Figure 16). The matrix is vesicular in places and contains scattered oxides. Plagioclase phenocrysts are well formed, subhedral to euhedral, and show no signs of zoning or resorption. The sharp contrast between coarse feldspar and fine matrix suggests that this clast may record a magma recharge or mixing event.

Figure 16, SEM image of Clast 5, a porphyritic basalt with large feldspar phenocrysts

Clasts 6, 8, 10, and 11 are mafic cumulates composed of Mg-rich olivine and orthopyroxene, with subordinate plagioclase. The clasts appear well preserved, with coarse granular texture visible in BSE imagery (Figure 17). No zoning, alteration rims, or fractures are observed within the clast, supporting its interpretation as a slowly cooled cumulate with limited postformational modification.

Figure 17, Clast 10, a mafic cumulate

Clast 9 is a coarse-grained, spinel-bearing gabbroic cumulate composed primarily of pyroxene and plagioclase, with a significant component of Cr-spinel (Figure 18). Cr-spinel occurs both as isolated grains and as inclusions within larger pyroxene crystals, forming a poikilitic texture in some areas. Pyroxene makes up the majority of the clast by volume, with plagioclase interstitially distributed. The preservation of cumulate layering and the abundance of spinel indicate that Clast 9 likely formed in a magmatic setting with high chromite saturation, potentially linked to a layered mafic intrusion in the lunar crust.

Figure 18, BSE image of Clast 9, a spinel-bearing gabbroic cumulate.

Clast 13 is a fine-grained felsic fragment containing abundant plagioclase phases (Figure 19). Phosphate phases occur in discrete interstitial zones and are highlighted by P-rich signatures in EDS maps. The clast lacks pyroxene and is texturally distinct from the mafic clasts in the sample. It shows no signs of deformation or brecciation and likely represents a late-stage evolved melt pocket or a partially melted feldspathic lithology. The absence of shock features further supports its preservation.

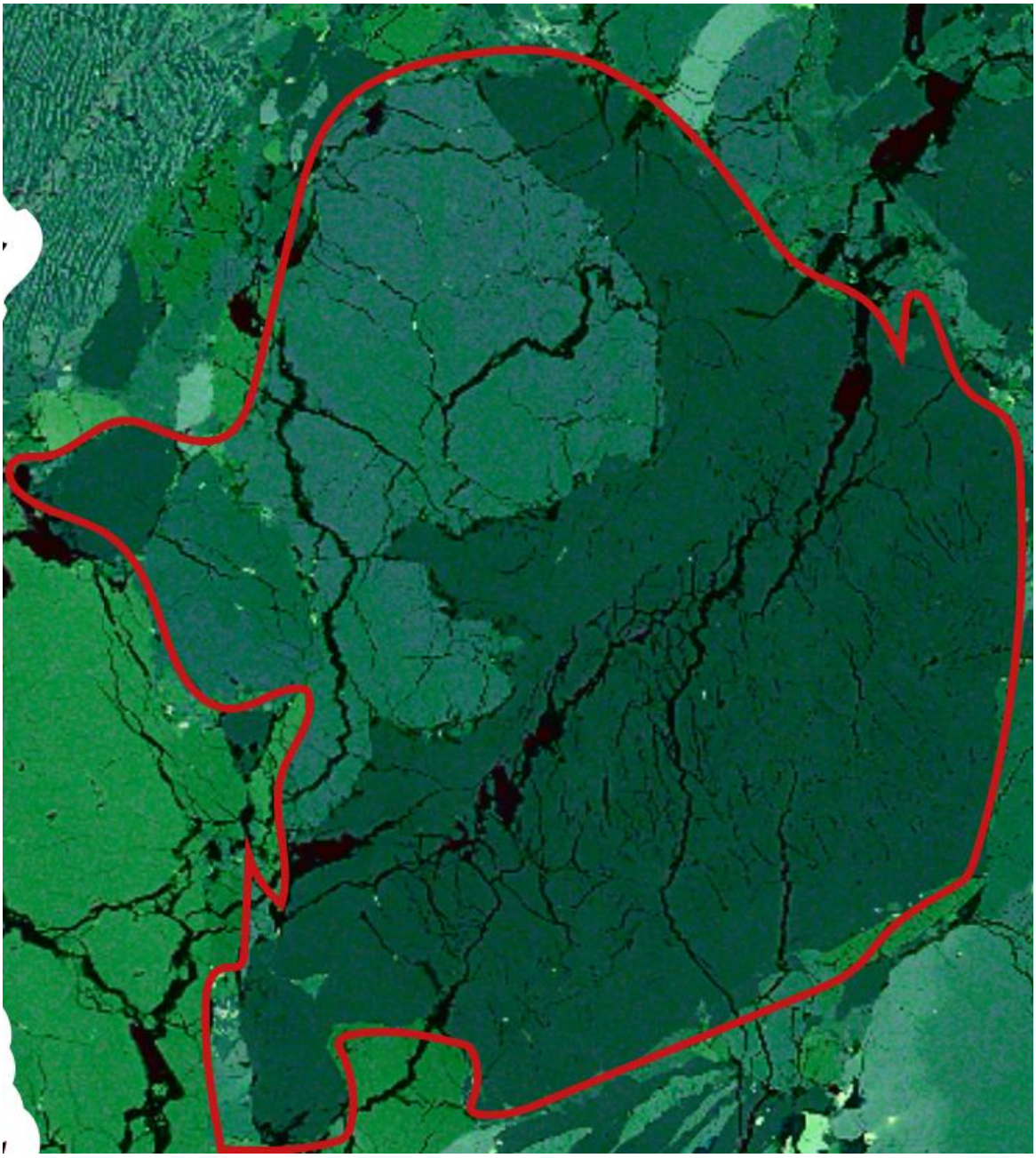

Figure 19, SEM image of Clast 13, rich in plagioclase phases

Clast 14 is a strongly altered basaltic fragment with irregular boundaries and multiple cross-cutting Ca- and P-rich veins (Figure 20). The outer margin shows a distinct alteration halo enriched in Fe oxides. The internal mineralogy includes feldspar and pyroxene, though much of the original texture is obscured by secondary phases. The pattern and chemistry of the veins suggest phosphate remobilization, either through low-temperature fluid interaction or late-stage thermal overprinting. This clast shows the clearest evidence of post-brecciation alteration in the section

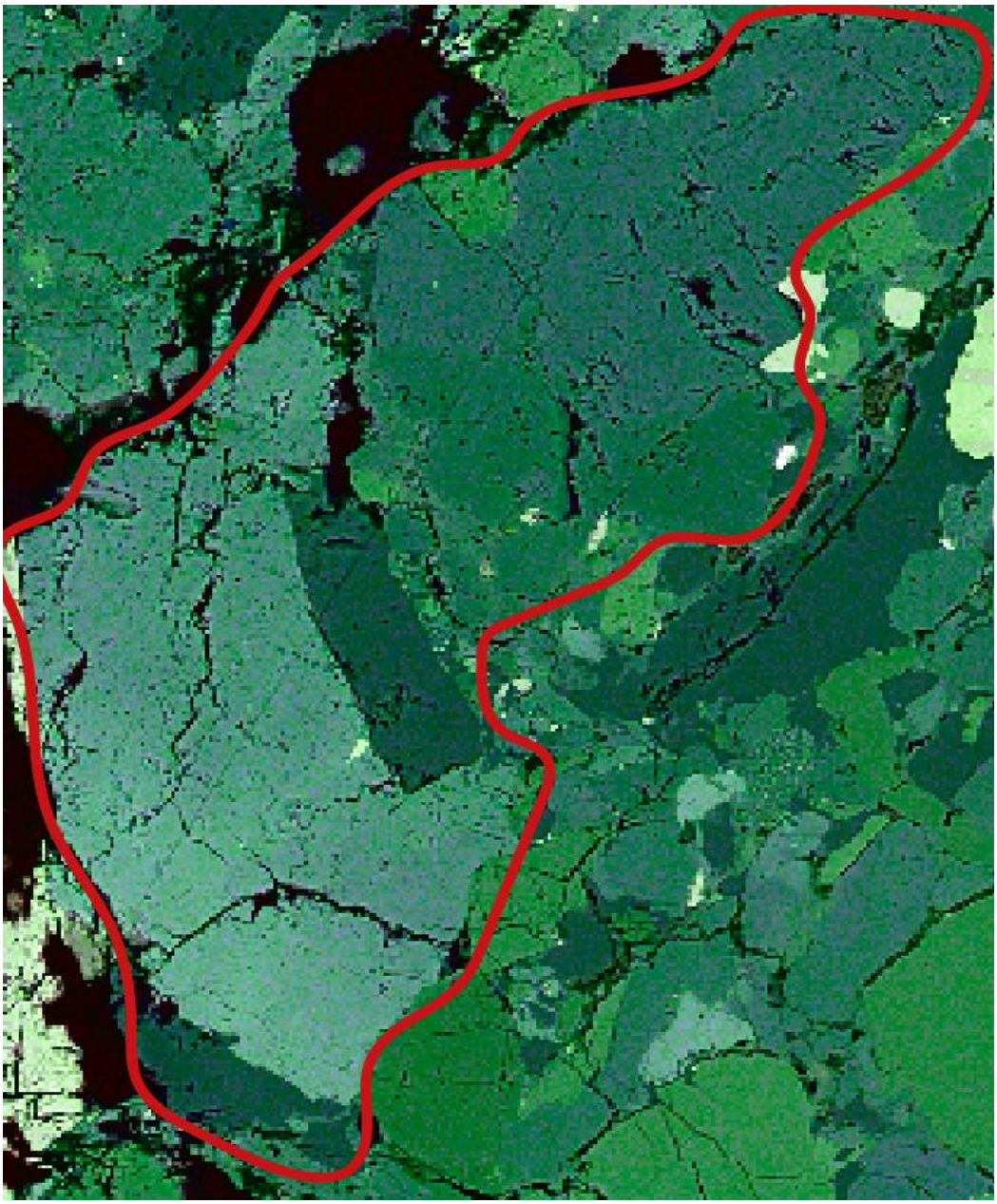

Figure 20, BSE image of Clast 14, an altered basaltic fragment.

EDS mapping (Figures 6–9) confirmed elemental zoning patterns across clasts and helped guide SIMS target selection. These maps were essential for isolating accessory minerals such as phosphates and feldspars, which were used in Pb-Pb dating.

Clast No.	**Rock Type**	**Dominant Mineralogy**	**Inferred Environment of Formation**
1	Subophitic basalt	Plagioclase, low-Ca pyroxene	Shallow basaltic lava or sill
2	Subophitic basalt	Plagioclase, Fe-Mg pyroxene	Extrusive basalt
3	Ti-rich evolved basalt	Ilmenite, titanomagnetite, pigeonite	Differentiated melt pocket
4	Subophitic basalt	Plagioclase, pyroxene	Lava flow with slow cooling
5	Porphyritic basalt	Feldspar phenocrysts, Fe-rich groundmass	Recharge/mixing in subvolcanic conduit
6	Mafic cumulate	Olivine, Mg-rich orthopyroxene	Deep crustal intrusion
7	Altered fragment	Fine plagioclase, minor oxides	Partially shocked feldspathic fragment
8	Mafic cumulate	Olivine, orthopyroxene	Primitive cumulate
9	Spinel-rich gabbro	Cr-spinel, plagioclase, pyroxene	Layered plutonic complex
10	Mafic cumulate	High-Mg pyroxene, olivine	Intrusive origin, mantle-derived melt
11	Mafic cumulate	Pyroxene, minor plagioclase	Early crystallizing cumulate
12	Vesicular basalt	Pyroxene, vesicles	Volcanic surface flow
13	Felsic fragment	Al-rich plagioclase, silica-rich mesostasis	Residual melt or evolved intrusive material
14	Altered basaltic clast	Ca-rich feldspar, Sc anomalies, oxide rims	Late-stage alteration/metasomatism

5.5 Isochron Dating Results

In this study, Clast 1, a subophitic basalt consisting primarily of plagioclase and Fe-Mg pyroxene, was selected for in situ SIMS Pb-Pb dating. This clast was chosen based on its pristine igneous texture, minimal alteration, and the presence of late-stage phosphate and potassium feldspar phases suitable for isotopic analysis. High-resolution SEM-EDS mapping identified numerous U- and Pb-bearing sites, including apatite and K-feldspar grains, which were targeted for SIMS analysis (Figure 21).

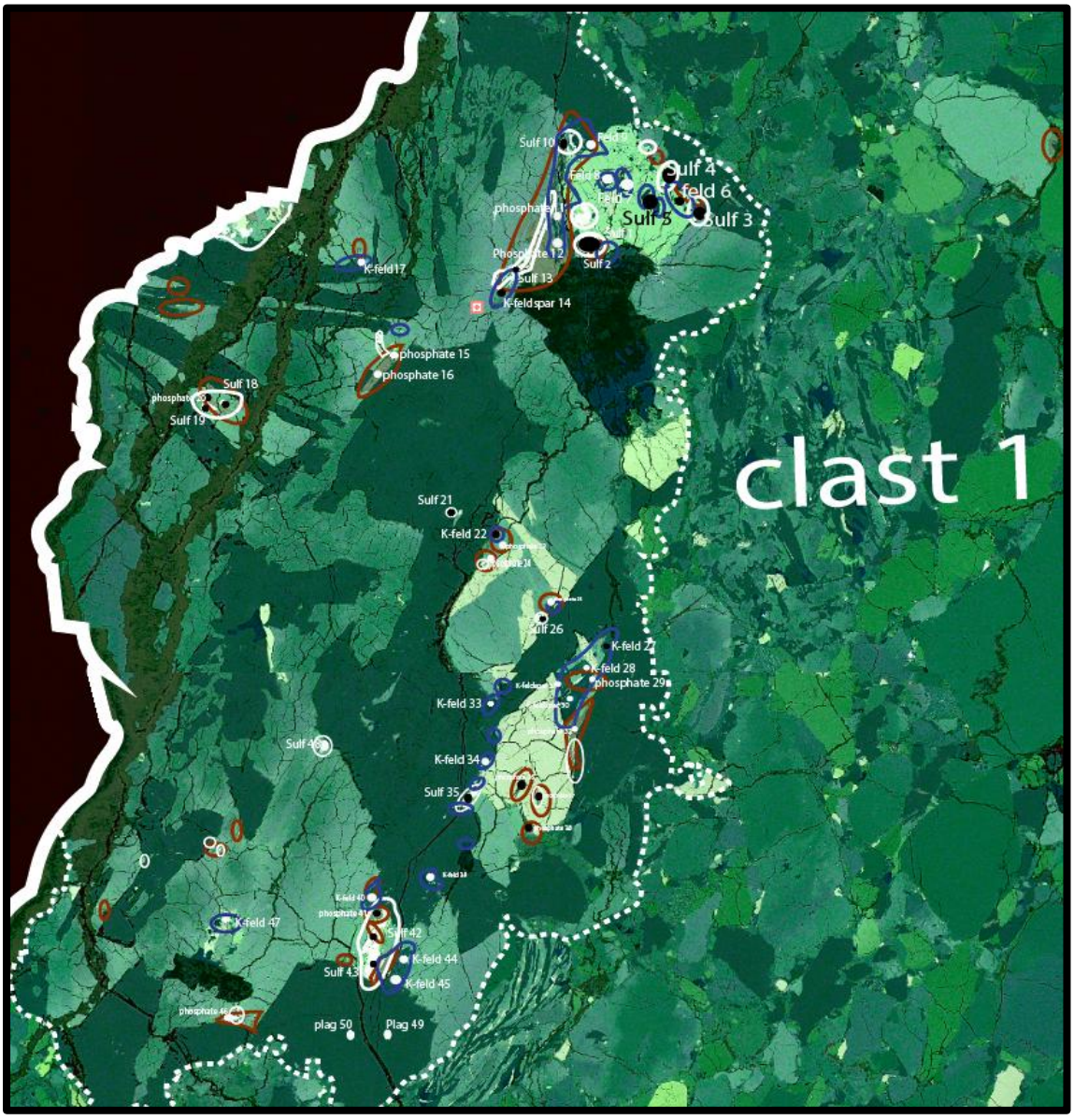

Figure 21, Elemental map of Clast 1 from NWA 12384, showing the distribution of key U- and Pb-bearing phases used for in situ SIMS Pb-Pb dating, with phosphates in red, potassium feldspar in blue, and sulfides in white.

An isochron was constructed based on Pb isotopic ratios ($^{204}Pb/^{206}Pb$ vs. $^{207}Pb/^{206}Pb$) obtained from in situ SIMS analyses on phosphate and feldspar grains within Clast 2, a subophitic basalt identified as minimally altered and texturally pristine (see Figure 13). This clast was selected due to its well-preserved primary igneous phases and high U-Pb elemental concentrations, which provided suitable conditions for robust isotopic dating (Yen et al., 2024).

The isochron regression was performed using the Isoplot 3.60 software (Ludwig, 2008), which incorporates both analytical uncertainties and data scatter. The result yielded a model $^{207}Pb/^{206}Pb$ age of 3219 ± 13 Ma. The calculated MSWD (Mean Square of Weighted Deviates) was 1.3, indicating that the scatter in the data is within acceptable limits for geological interpretation and consistent with a single, well-constrained crystallization event.

To correct for potential common Pb, the data were referenced against the Stacey and Kramers (1975) terrestrial Pb evolution model. Data points showing evidence of mixing or contamination were excluded from the regression. The robustness of the isochron is evident from its linear array and low analytical scatter, supporting the interpretation of this age as the crystallization age of Clast 2.

This age places the basalt firmly within the Late Imbrian epoch, consistent with prior SIMS-based dating of other lunar meteorites, including NWA 4734 (Merle et al., 2020) and LAP 02205 (Snape et al., 2016). These results support an emerging view that lunar magmatic activity persisted beyond the major period of mare basalt emplacement recorded by Apollo samples, which largely range from ~3900 to ~3300 Ma (Hiesinger et al., 2011).

The regression line and data distribution are shown in Figure 22, including 95% confidence intervals and labeled error ellipses. These results strengthen the interpretation of localized magmatic provinces active during the waning stages of lunar volcanism.

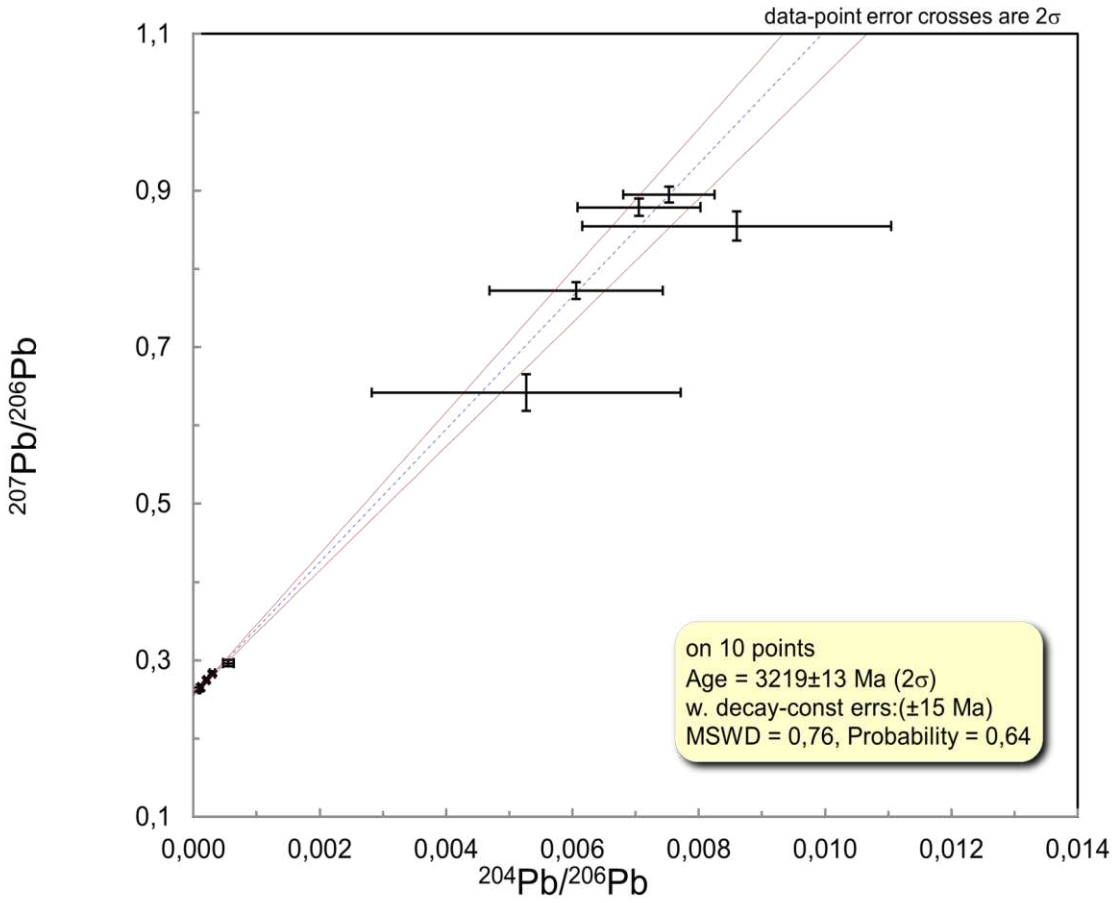

Figure 22, Pb-Pb isochron plot for Clast 2, based on SIMS analyses of phosphate and potassium feldspar grains. The regression yields a crystallization age of 3219 ± 13 Ma

6. Discussion

6.1 Implication for lunar volcanism

The petrographic and geochemical variability observed among clasts in NWA 12384 provides compelling evidence for a prolonged and heterogeneous magmatic history on the Moon. The coexistence of primitive mafic fragments, evolved basaltic rocks, and felsic clasts within a single breccia sample suggests multiple generations of volcanic activity, each derived from distinct mantle sources and crystallization regimes (Yen et al., 2024; Papike et al., 1998).

The most direct evidence comes from Clast 1, a subophitic basalt selected for in situ SIMS dating due to its pristine igneous texture and preservation of primary phosphate and feldspar phases (Figure 13; Table 1). The resulting crystallization age of 3219 ± 13 Ma confirms magmatic activity during the Late Imbrian epoch, well beyond the timeframe recorded by Apollo mare basalts, which mostly range from 3900 to 3300 Ma (Hiesinger et al., 2011).

The Fe-Ti oxide enrichment in other clasts points to late-stage magmatic differentiation, while the presence of Mg-rich cumulates reflects early high-temperature crystallization. This diversity supports models of localized and long-lived mantle heat sources, such as KREEP-enriched reservoirs, capable of sustaining partial melting over extended periods (Snape et al., 2016; Merle et al., 2020).

These findings, anchored by the age of Clast 1, affirm the role of meteorites like NWA 12384 in refining lunar volcanic chronology. They offer evidence that magmatism was not globally synchronous but instead evolved through spatially and temporally isolated events across the lunar crust.

6.2 Regolith formation and brecciation

The regolith-related features preserved in NWA 12384 offer valuable insights into the cumulative effects of meteoritic bombardment on the lunar surface and the formation of polymict breccias. The matrix of NWA 12384 contains fine-grained lithic debris, recrystallized fragments, and glassy melt pockets, all indicative of multiple impact events and surface reworking processes (Joy & Arai, 2013; Papike et al., 1998),

The SIMS-derived Pb-Pb age of 3219 ± 13 Ma was obtained from Clast 1, a subophitic basalt composed of intergrown plagioclase and Fe-Mg pyroxenes (see Table 1, Figure 13). This clast

likely crystallized from a relatively evolved magma under moderate cooling conditions, possibly in a shallow intrusive setting such as a sill or subsurface lava flow. Its well-preserved igneous texture and mineralogy made it an ideal target for isotopic analysis.

This age places the basalt firmly in the Late Imbrian epoch and significantly postdates the dominant phase of mare basalt emplacement recorded by Apollo samples (~3900–3300 Maa) (Hiesinger et al., 2011). It aligns with results from other meteorites such as NWA 4734 and LAP 02205, which also preserve Late Imbrian crystallization ages (Merle et al., 2020; Snape et al., 2016).

The breccia's matrix features, including clast fragmentation, melt veining, and partial recrystallization, reflect repeated impact gardening and regolith processing, likely occurring during or shortly after the emplacement of Clast 1. These conditions suggest that volcanic activity and surface modification were overlapping phenomena in this portion of the lunar crust.

As shown in Figure 23, the crystallization age of Clast 1 fits within a cluster of similarly aged meteorites, indicating that volcanic and regolith-forming processes were active across multiple lunar regions during the Late Imbrian.

Taken together, these observations reinforce the value of polymict breccias as time-resolved records of both volcanic and impact-related evolution in the upper lunar crust.

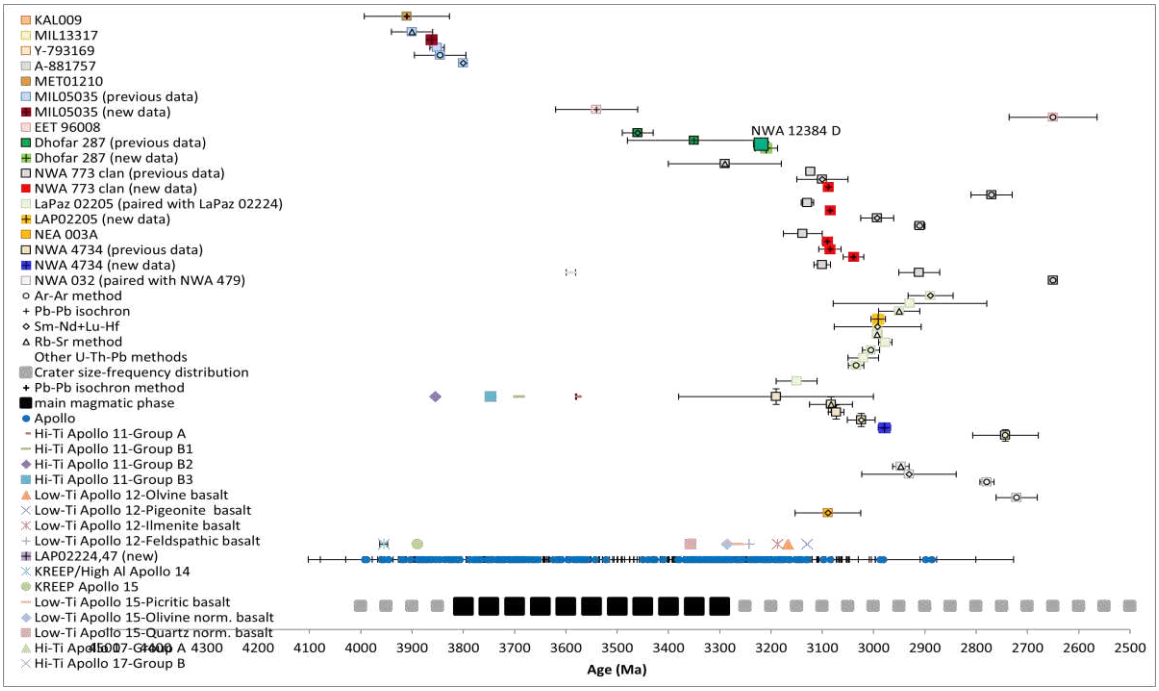

Figure 23, Plotting of the age of NWA 1384 (large green square) compared to other meteorites, The large black squares bar at the bottom of the graph represent the main age range (~3900–3200 Ma) of mare basalt samples returned by the Apollo missions. (modified from Merle et al., 2020)

6.3 Comparison to Apollo Samples

The crystallization age obtained from Clast 1 in this study, 3219 ± 13 Ma, falls significantly outside the main age distribution of mare basalts returned by the Apollo missions, which generally range from ~3.9 to 3.3 billion years ago (Hiesinger et al., 2011). This discrepancy underscores the limitations of mission-constrained sampling and highlights the complementary value of lunar meteorites for extending the known duration of lunar volcanism.

Apollo samples, while geochemically diverse, originate from geographically limited regions on the nearside of the Moon. As a result, their collective age spectrum is biased toward early mare emplacement and does not capture the full extent of localized magmatic activity that may have persisted in more isolated or KREEP-rich regions of the crust (Shearer & Papike, 1999). In contrast, meteorites like NWA 12384 provide a more randomized, regolith-integrated record of crustal processes from unknown lunar provenances (Joy & Arai, 2013).

The SIMS-derived age from Clast 1 adds to a growing number of meteorite-based studies documenting volcanic activity well into the Late Imbrian epoch, alongside examples such as NWA 4734 (~3200 Ma) and LAP 02205 (~2950 Ma) (Merle et al., 2020; Snape et al., 2016). These findings support the view that lunar magmatism did not cease abruptly after ~3300 Ma but instead tapered gradually in localized provinces, driven by residual heat and possibly isolated magmatic systems.

This pattern is clearly illustrated in Figure 24, which shows two main peaks in the age distribution of lunar volcanic samples: an older episode around 3900–3600 Ma and a younger, extended volcanic phase spanning 3300–3000 Ma. The age of Clast 1 from NWA 12384 falls near the center of this younger peak, reinforcing the interpretation that late-stage volcanic activity was both real and geochemically significant.

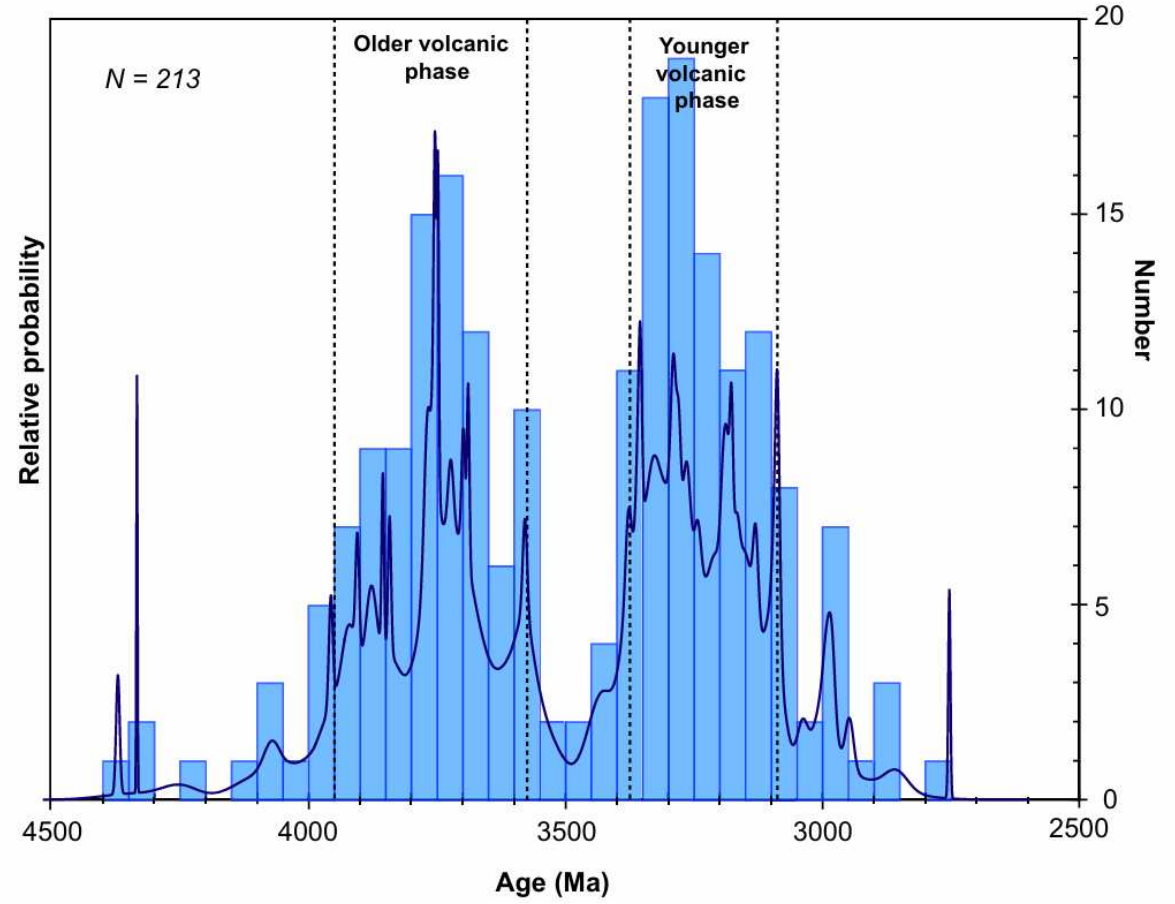

Figure 24, Histogram showing the distribution of crystallization ages from lunar volcanic samples, from Merle et al.,2020

6.4 Broader implication for Lunar chronology

The crystallization age obtained from Clast 1 in NWA 12384, 3219 ± 13 Ma, has broader implications beyond the immediate interpretation of this individual basalt. It contributes to a growing dataset of lunar meteorites that reveal volcanic activity extending hundreds of millions of years beyond the age range of Apollo basalts. When placed in the context of lunar evolution, this age challenges the notion of a rapid thermal shutdown and instead supports models of prolonged, regionally sustained magmatism (Merle et al., 2020; Snape et al., 2016; Hiesinger et al., 2011).

This finding aligns with recent interpretations of Pb-Pb and Ar-Ar ages from other lunar meteorites, many of which cluster around the 3.2 to 2.9 Ga window. These ages suggest that late-stage volcanic activity may have been common in isolated provinces, possibly linked to residual KREEP-rich mantle domains or crustal heat retention in low-conductivity terrains (Shearer & Papike, 1999; Jolliff et al., 2000).

Crucially, the age of Clast 1 helps fill a relative gap between the oldest lunar basalts (>3.8 Ga) and the youngest known volcanic products (~1.2 Ga from crater counts and rare Ar-Ar dates). It adds to the cumulative statistical weight of lunar meteorite data suggesting that volcanic frequency peaked early, declined gradually, and persisted regionally through the Imbrian and possibly into the Eratosthenian period (Hiesinger et al., 2011; Joy & Arai, 2013).

The contribution of meteorites like NWA 12384, especially those that preserve datable, minimally altered clasts such as Clast 1, is essential for reconstructing a more continuous lunar magmatic timeline. These breccias act as natural samplers of crustal processes, integrating events across both space and time in a way that no single landed mission can.

7. Conclusion

This study presents a detailed petrographic, geochemical, and isotopic investigation of the lunar meteorite NWA 12384, with the goal of refining our understanding of late-stage lunar magmatism and regolith evolution. Through SEM and EDS analyses, fourteen lithic clasts were classified into a range of igneous types, including subophitic basalts, Fe-Ti oxide-rich fragments, mafic cumulates, and evolved felsic materials. This lithological diversity reflects contributions from multiple magmatic episodes, each with distinct thermal and chemical histories.

The most significant result was obtained from Clast 1, a well-preserved subophitic basalt, which yielded a crystallization age of 3219 ± 13 Ma based on in situ Pb-Pb isotopic dating using SIMS. This Late Imbrian age adds to a growing body of evidence that volcanic activity on the Moon continued far beyond the major mare-forming period recorded by Apollo samples. It also supports models of localized, long-lived heat sources capable of sustaining magmatism in specific crustal domains.

The features preserved in NWA 12384, such as melt veins, impact textures, and clast heterogeneity, further illustrate the interplay between volcanism and regolith processing during lunar history. This breccia captures both volcanic and impact-driven processes, offering a stratified archive of the Moon's crustal evolution.

By integrating petrography, elemental mapping, and precise isotopic dating, this study demonstrates the scientific value of lunar meteorites in filling gaps left by sample-return missions. In particular, the age and characteristics of Clast 1 provide a key datapoint for extending the lunar magmatic timeline and contextualizing the spatial heterogeneity of lunar evolution.

Acknowledgements

Firstly I want to thank my Supervisor, Renaud, who allowed me to take part in this project and helped me through it all, made me experience first hand the working of SIMS and EDS analysis, and has been infinitely patient despite my sometimes frustrating disorganization.

To my Co-relator Mara Murri a sincere thank you, not only for helping me reach this achievement, but also for all the aid given to me during this past year and a half, both in and out of the country.

I also want to thank my family, my mom and dad, my brother and my grandmother, who allowed me to experience this wonderful semester abroad, and which despite being so far apart, have been so close to me in these months.

References

1. **CAMECA. (n.d.).** ***SIMS: Secondary Ion Mass Spectrometry technique.*** **https://www.cameca.com/products/sims/technique, May 5, 2025**
2. **CAMECA**. *EPMA: Electron Probe MicroAnalyzer Introduction*. https://www.cameca.com/products/epma/epma-introduce, **May 5, 2025**
3. **Hiesinger H., Head, J. W. III, Wolf, U., Jaumann, R., & Neukum, G.** (2011). Ages and stratigraphy of lunar mare basalts: A synthesis. In W. A. Ambrose & D. A. Williams (Eds.), *Recent Advances and Current Research Issues in Lunar Stratigraphy* (Geological Society of America Special Paper 477, pp. 1–51). https://doi.org/10.1130/2011.2477(01)
4. **Irving, A. J., & Kuehner, S. M.** (2019). *Northwest Africa 12384 (NWA 12384)*. The Meteoritical Bulletin, No. 109. Meteoritical Society. Retrieved from https://www.lpi.usra.edu/meteor/metbull.php?code=71235
5. **Joy, K. H., & Arai, T.** (2013). Lunar meteorites: New insights into the geological history of the Moon. *Astronomy & Geophysics*, 54(4), 4.28–4.32.
6. **Ludwig, K. R.** (2008). *User's manual for Isoplot 3.60: A geochronological toolkit for Microsoft Excel*. Berkeley Geochronological Center Special Publication No. 4. Berkeley, California: Berkeley Geochronological Center.
7. **Merle, R. E., et al.** (2020). Pb-Pb ages and initial Pb isotopic composition of lunar meteorites: NWA 773 clan, NWA 4734, and Dhofar 287. *Meteoritics & Planetary Science*, 55(8), 1808–1832. https://doi.org/10.1111/maps.13547
8. **Norman, M. D.** (2009). The Lunar Cataclysm: Reality or Mythconception? *Elements*, 5(1), 23–28.
9. **Ortega, E., Hosseinian, H., Rosales López, M. J., Rodríguez Vera, A., & Hosseini, S.** (2022). Characterization Techniques for Chemical and Structural Analyses. In *Advanced Functional Materials* (pp. [chapter pages]). https://doi.org/10.1007/978-981-16-9569-8_4
10. **Papike, J. J., Ryder, G., & Shearer, C. K.** (1998). Lunar Samples. In *Planetary Materials* (pp. 5-1–5-234). Mineralogical Society of America.

11. **Snape, J. F., Nemchin, A. A., Bellucci, J. J., Whitehouse, M. J., Tartèse, R., Barnes, J. J., Anand, M., Crawford, I. A., & Joy, K. H.** (2016). Lunar basalt chronology, mantle differentiation and implications for determining the age of the Moon. *Earth and Planetary Science Letters*, 451, 149–158. https://doi.org/10.1016/j.epsl.2016.07.026
12. **Stacey, J. S., & Kramers, J. D.** (1975). Approximation of terrestrial lead isotope evolution by a two-stage model. *Earth and Planetary Science Letters*, 26, 207–221.
13. **Yen, C. J.-K., Carpenter, P. K., Deligny, C., Nemchin, A., Merle, R., Irving, A. J., Nishiizumi, K., Caffee, M. W., Jull, A. J. T., Whitehouse, M., & Jolliff, B. L.** (2024). Petrology and chronology of mare components in lunar basaltic breccia meteorite Northwest Africa 12384. *Meteoritics & Planetary Science*, 59(4), e21441. https://doi.org/10.1111/maps.14260